Published in final edited form as:
Nanomedicine (Lond). 2015 ; 10(7): 1111–1125. doi:10.2217/nnm.14.170.

Fluorophore-labeling of core-crosslinked polymeric micelles for multimodal in vivo and ex vivo optical imaging

Yang Shi[1], **Sijumon Kunjachan**[2], **Zhuojun Wu**[2,3,4], **Felix Gremse**[2], **Diana Moeckel**[2], **Marc van Zandvoort**[3,4], **Fabian Kiessling**[2], **Gert Storm**[1,5], **Cornelus F. van Nostrum**[1], **Wim E. Hennink**[1], and **Twan Lammers**[1,2,5,*]

[1]Department of Pharmaceutics, Utrecht Institute for Pharmaceutical Sciences (UIPS), Utrecht University, Utrecht, The Netherlands [2]Department of Experimental Molecular Imaging (ExMI), Helmholtz Institute for Biomedical Engineering, RWTH Aachen University Clinic, Aachen, Germany [3]Institute for Molecular Cardiovascular Research (IMCAR), RWTH Aachen University Clinic, Aachen, Germany [4]Department of Genetics and Cell Biology, Cardiovascular Research Institute Maastricht (CARIM), Maastricht University, Maastricht, The Netherlands [5]Department of Controlled Drug Delivery, MIRA Institute for Biomedical Technology and Technical Medicine, University of Twente, Enschede, The Netherlands

Abstract

Aim—To enable multimodal *in vivo* and *ex vivo* optical imaging of the biodistribution and tumor accumulation of core-crosslinked polymeric micelles (CCPM).

Materials & Methods—mPEG-b-p(HPMAm-Lac)-based polymeric micelles, core-crosslinked via cystamine and covalently labeled with two fluorophores (Dy-676/488) were synthesized. The CCPM were intravenously injected in CT26 tumor-bearing mice.

Results—Upon intravenous injection, the CCPM accumulated in CT26 tumors reasonably efficiently, with values reaching ~4 %ID at 24 hours. *Ex vivo* TPLSM confirmed efficient extravasation of the iCCPM out of tumor blood vessels and deep penetration into the tumor interstitium.

Conclusions—CCPM were labeled with multiple fluorophores, and they exemplify that combining different *in vivo* and *ex vivo* optical imaging techniques is highly useful for analyzing the biodistribution and tumor accumulation of nanomedicines.

Keywords

Nanomedicine; Drug targeting; Optical imaging; Theranostics; Micelles; pHPMA; PEG

1. INTRODUCTION

Nanomedicine, i.e. the application of nanotechnology to healthcare, has received considerable attention recent years, in particular for the diagnosis and treatment of cancer.

*Corresponding author: tlammers@ukaachen.de.

Europe PMC Funders Author Manuscripts

[1-3] The impact of nanotechnology on medicine ranges from the solubilization of hydrophobic compounds and the stabilization of biopharmaceuticals, to the targeted delivery of therapeutic payloads to pathological sites. Tumor-targeted drug delivery is generally based on the Enhanced Permeability and Retention (EPR) effect, which enables the accumulation of ~1-100 nm-sized long-circulating drug carriers in tumors, while preventing their localization in potentially endangered healthy tissues.[4-7].

Among the large number of tumor-targeting nanomedicines designed and evaluated to date, polymeric micelles are one of the most prominent and most successful systems.[8-11] Polymeric micelles consist of a hydrophobic core and a hydrophilic stealth corona. This stealth corona is key for assuring long circulation times upon intravenous (i.v.) administration. The size of polymeric micelles is generally below 100 nm, and this small size not only assures prolonged circulation times, but also efficient extravasation and penetration at the target site. Because of the flexibility of polymer chemistry, micelle-forming polymers can be modified with various reactive groups, which can be further functionalized with drugs, drug linkers, imaging agents and targeting moieties. Moreover, polymeric micelles can be chemically and/or physically crosslinked, to increase their colloidal stability and their circulation times.[12-14] And furthermore, thermosensitive polymeric micelles, a special type of micelles formed using temperature-responsive amphiphilic block copolymers, are of great interest for targeted drug delivery purposes, because of their facile and robust micelle-formation process.[15-18]

In recent years, significant efforts have been invested in visualizing and quantifying the biodistribution and the target site accumulation of nanomedicines using non-invasive imaging techniques.[19-23] Several different modalities, including positron emission tomography (PET), single photon emission computed tomography (SPECT), magnetic resonance imaging (MRI), X-ray computed tomography (CT), ultrasound (US) and optical imaging (OI), have been employed for such purposes.[24-27] Compared to other available techniques, OI has recently gained significant attention, because of its user-friendliness, its time- and cost-effectiveness, and its ability to be used for high-throughput screening. Two-dimensional fluorescence reflectance imaging (2D FRI) is the most popular OI technique, but issues related to poor light penetration and difficult quantification limit its *in vivo* application, in particular in case of whole body biodistribution imaging, which goes beyond the visualization of nanomedicine accumulation in superficial tumors. Three-dimensional fluorescence molecular tomography (3D FMT) can partially overcome these issues. However, the ability of 3D FMT to accurately assign fluorescence signals to internal organs and deeper-seated tissues is limited, because of the lack of anatomical information. The latter shortcoming can be resolved by employing micro-computed tomography (CT), and by fusing and reconstructing the obtained FMT data sets with the information obtained using CT. The resulting technique, i.e. hybrid CT-FMT, has recently been shown to be useful for non-invasively visualizing and quantifying the biodistribution and the tumor accumulation of fluorophore-labeled polymeric nanocarriers.[28, 29]

We here aimed to synthesize core-crosslinked polymeric micelles (CCPM) based on thermosensitive block copolymers, and we labeled them with two different fluorophores (Dy-488 and Dy-676), to enable multimodal optical imaging. The near-infrared fluorophore

(NIRF) Dy-676 was used for in vivo FRI and CT-FMT, while the standard fluorophore Dy-488 was employed for ex vivo histological validation of tumor accumulation and penetration using 2D fluorescence microscopy (FM) and 3D two-photon laser scanning microscopy (TPLSM). If integrated into a single experimental setup, the combination of such *in vivo* and *ex vivo* optical imaging techniques can provide a wealth of information of the biodistribution and the target site accumulation of (double-labeled) CCPM, and it is consequently considered to be highly useful for translational nanomedicine research.

In the present manuscript, a novel type of image-guided core-crosslinked polymeric micelle (iCCPM) formulation was prepared, enabling double-labeling with two different fluorophores. The motivation for developing a novel synthetic protocol for synthesizing iCCPM is based on the notion that the previously established strategy for core-crosslinking mPEG-b-p(HPMAm-Lac$_n$) block copolymers - i.e. the radical polymerization of methacrylate-containing side groups in the micellar core [30-32] - turned out to be incompatible with the two fluorophores used, resulting in a loss of their optical properties. Here, we therefore synthesized a mPEG-b-p(HPMAm-Lac)-based block copolymer with acrylic acid N-hydroxysuccinimide (ANHS) ester repeating units in the thermosensitive block. Such reversibly crosslinked polymeric micelles responsive to reductive environments have been shown to present with good in vivo antitumor efficacy [33-36], but this type of core-crosslinking has not yet been used to enable fluorophore labeling and multimodal optical imaging of the biodistribution and the tumor accumulation of CCPM. The polymeric micelles were based on p(HPMAm), which were shown to be safe and biocompatible. [37-41] Dy-488 and Dy-676 were conjugated to the micellar core, which mimics drug loading in micelles. Moreover, the important surface properties of the micelles, e.g., PEG chain flexibility, hydrophilicity and charge, are not changed by this strategy. Upon i.v. injection, schematically shown in Scheme 1, the double-labeled iCCPM showed a reasonable degree of EPR-mediated tumor accumulation (~4% of the injected dose), but also relatively high amounts present in liver and kidney, which can be ascribed to MPS-mediated clearance and to the presence of several free polymer chains in the final micellar formulation, respectively. Double-labeling of the micelles not only enabled assessment of tumor accumulation and off-target localization at the whole organism level using 2D FRI and 3D CT-FMT, but also allowed for a detailed assessment of their extravasation and penetration at the microscopic level. Consequently, our findings demonstrate that the covalent entrapment of two different fluorophores within core-crosslinked polymeric micelles is possible, and they indicate that such double-labeled nanomedicine formulations are highly useful for multimodal *in vivo* and *ex vivo* optical imaging of their biodistribution and target site accumulation.

2. MATERIALS AND METHODS

2.1. Materials

The mPEG$_2$-ABCPA macroinitiator (M_n of mPEG = 5000 g·mol^{-1}) and *N*-(2-hydroxypropyl) methacrylamide monolactate (HPMAm-Lac) were prepared according to previously published procedures.[30] Acrylic acid N-hydroxysuccinimide ester (ANHS) and cystamine dihydrochloride were purchased from Sigma-Aldrich. Amino-functionalized

Dy-488 (absorption and emission maxima: 491 nm and 515 nm; in PBS 7.4) and Dy-676 (absorption and emission maxima: 674 nm/699 nm; in ethanol) were ordered from Dyomics.

2.2. Synthesis of *ω*-methoxy poly(ethylene glycol)-*b*-(*N*-(2-hydroxyethyl)methacrylamide)-monolactate)-*co*-(acrylic acid *N*-hydroxysuccinimide ester)

The block copolymer mPEG-*b*-p(HPMAm-Lac-*co*-ANHS was synthesized by free radical polymerization using HPMAm-Lac and ANHS as comonomers, and $mPEG_2$-ABCPA as macroinitiator (Scheme 1A).[16] The reagents were dissolved in DMSO at a monomer concentration of 300 mg/mL. The molar ratio of monomer-to-macroinitiator was 150/1, and that of HPMAm-Lac and ANHS was 4/1. Reactions were conducted at 70 °C for 24 h under a nitrogen atmosphere. The polymer was purified by precipitation in diethyl ether, and then dissolved in cold reverse osmosis (RO) water and dialyzed against RO water at 4 °C for 24 h. The polymer was collected as a fluffy white powder after freeze-drying.

2.3. Characterization of mPEG-*b*-p(HPMAm-Lac-*co*-ANHS) by ^{1}H NMR and GPC

The ^{1}H NMR spectra were recorded using a Gemini 300 MHz spectrometer (Varian Associates Inc. NMR Instruments, Palo Alto, CA), using d6-DMSO as the solvent; the DMSO peak at 2.5 ppm was used as the reference line. ^{1}H NMR of mPEG-*b*-p(HPMAm-Lac-*co*-ANHS): 7.3 (b, CO-N<u>H</u>-CH_2), 5.2 (b, CH(CH_3)-O<u>H</u>), 4.8 (b, NH-CH_2-C<u>H</u>(CH_3)-O-(Lac)), 4.1 (b, C<u>H</u>(CH_3)-OH), 3.4–3.6 (b, mPEG5000 methylene protons, O-CH_2-CH_2), 2.8 (b, CH2-CH2 from the NHS groups), 0.6-3.2 (b, the rest of the protons are from the methyl and backbone CH_2 protons). The polymer composition was evaluated by ^{1}H NMR as follow: (I) number of the HPMAm-Lac repeating units: in the ^{1}H NMR spectrum of the purified polymer, the integral at 3.4-3.6 ppm of methylene protons of $mPEG_{5000}$ was set as 448 (the average number of protons per one mPEG chain, M_n=5000), and the integral value of the chemical shift at 4.1 ppm is assigned to the HPMAm-Lac repeating units.[16] (II) number of the ANHS repeating units: The mole fraction of vinyl protons of ANHS at 6.3 and 6.6 ppm relative to methylene protons of $mPEG_{5000}$ at 3.4-3.6 ppm in the crude product after polymerization was compared to that before the polymerization. GPC was conducted to determine the number average molecular weight (M_n), weight average molecular weight (M_w) and polydispersity (PDI, equal to M_w/M_n) using two serial Plgel 5 μm MIXED-D columns (Polymer Laboratories) and PEGs of narrow molecular weight distribution as calibration standards. The eluent was DMF containing 10 mM LiCl, the elution rate was 0.7 mL/min and the temperature was 40 °C. [16]

2.4. Conjugation of Dy-490 and Dy-676 to mPEG-b-p(HPMAm-Lac-co-ANHS)

The conjugations were performed following a previously published procedure.[42] Briefly, as exemplified by Scheme 2B-C, 0.15 mL of Dy-676 or Dy-488 stock solution (0.67 mg/mL) in DMSO (dried on molecular sieves A4) and 25 mg of the polymer were transferred into a dried two-necked flask. One equivalent of TEA to Dy-488 was added to the reaction mixture. The reaction mixtures were kept at 50 °C with stirring. To analyze the coupling efficiency, samples from the reaction mixtures were diluted 20 times with DMF (10 mM LiCl) and analyzed by GPC (method described in section 2.3) equipped with a UV detector. The detection wavelengths for Dy-676 and Dy-488 were 685 and 320 nm (since the

488 nm signal could not be clearly delineated in DMF), respectively. Dy-676 and Dy-488 solutions in DMF containing 10 mM LiCl ranging from 0.001 to 0.2 mg/mL were injected as calibration standards. After reaction for 96 h, the polymers were precipitated in diethyl ether for three times and then dried in vacuum at 25 °C.

2.5. Preparation and characterizations of fluorophore-labeled mPEG-b-p(HPMAm-Lac-co-ANHS) polymeric micelles

Polymeric micelles were prepared by the rapid heating protocol.[15, 16, 43] In short, mPEG-b-p(HPMAm-Lac-co-ANHS) was dissolved at 0 °C in PBS 7.4 at a concentration of 10 mg/mL. Next, the polymer solutions were heated to 50 °C in a water bath for 1 min under vigorous shaking, to form the micelles. The CCPM were prepared by adding cystamine dihydrochloride in PBS 7.4 (96 mg/mL) to the micellar suspension (the feed ratio of cystamine dihydrochloride/NHS ester groups was 1/2). The mixture was gently vortexed for a 30 s and incubated at 37 °C for 20 h.[44-46] The iCCPM were prepared using a mixture of equal amounts of the polymers modified with Dy-488 and Dy-676 (see Section 2.4 and 3.2; on average, 3.1 and 3.8% of the polymer chains were labeled with one molecule of Dy-488 or Dy-676) using the same protocol as for the CCPM. The iCCPM were purified by Vivaspin centrifugal concentrators (four times; membrane cut-off 10 kDa), to remove traces of the non-conjugated free fluorophores. The amount of free Dy-488 and Dy-676 in the filtrates was detected by HPLC (eluent A: water/ACN (95/5, v/v) with 0.1% perchlorate acid, eluent B: water/ACN (5/95, v/v) with 0.1% perchlorate acid; a gradient method with the volume fraction of eluent B increasing from 0 to 100% in 15 min; Sunfire C18 column and detection at 488 nm for Dy-488 and 654 nm for Dy-676). Subsequently, the volume of the micellar dispersion was decreased by a factor of four. The iCCPM were stored at −20 °C before further analysis and *in vivo* injection. The size of CCPM was measured by dynamic light scattering (DLS), using a Malvern 4700 system (Malvern Ltd., Malvern, U.K.) consisting of an Autosizer 4700 spectrometer, a pump/filter unit, a model 2013 air-cooler argon ion laser (75 mW, 488 nm, equipped with a model 2500 remote interface controller, Uniphase), a water bath, and a computer with DLS software (PCS, version 3.15, Malvern). Autocorrelation functions were analyzed by the cumulants method (fitting a single exponential to the correlation function to obtain the mean size and the polydispersity) and the CONtIN routine (fitting a multiple exponential to the correlation function to obtain the distribution of particle sizes). The measurement angle was 90°. The zeta potential of iCCPM was measured using a Malvern Zetasizer Nano-Z(Malvern Instruments, Malvern, UK) with universal ZEN 1002 dip cells and DTS (Nano) software (version 4.20) at 25 °C. Zeta potential measurements were performed in 20 mM HEPES pH 7.4 at a polymer concentration of 1 μg/mL. The size and fluorescent emission spectra of the iCCPM were characterized by nanoparticle tracking analysis (NTA)[30] and a Horiba Fluorolog fluorometer at 37 °C.[16]

2.6. Stability and reduction-sensitive de-crosslinking of the CCPM

The thermal stability of CCPM was studied by temperature-dependent DLS measurements. The size (Z_{ave}) and light scattering intensity (LSI) of the micelles were monitored by DLS while cooling a micellar suspension from 25 to 2 °C in 90 min.[15] Hydrolytic stability was analyzed by monitoring the Z_{ave} and the LSI of the micelles with DLS under accelerated

hydrolytic conditions (pH 10.0 and 37 °C) for 22 h.[16, 47, 48] The pH of the micellar dispersion was adjusted to pH 10.0 by diluting the micellar dispersion 5-fold with 500 mM Na_2CO_3/$NaHCO_3$ pH 10.0 buffer. The integrity of the CCPM against the dissolution by DMF was performed and also to examine the amount of non-crosslinked free polymer chains in the CCPM dispersion. The CCPM were freeze-dried and DMF (plus 10 mM LiCl) was added to the dry powder and the mixture was incubated for 5 h at 37 °C. The non-crosslinked polymeric micelles (NCPM) were treated similarly and the samples were subjected to GPC analysis as described in section 2.3. The de-crosslinking of the CCPM under reductive condition was performed as follows. The CCPM were incubated at pH 10.0 and 37 °C for 22 hours to hydrolyze the pendent hydrophobic groups in the micellar core. DTT, which is a commonly used reducing agent at the concentration of 5 mM to cleave disulfide bonds [49], was added in the micellar suspension and the mixture was generally vortexed for 1 min, and the Z_{ave} and LSI of the particles were monitored by DLS at 37 °C. [50] The CCPM were incubated with 5 mM DTT for 24 hours at 37 °C. The resulted dispersion was freeze-dried and dissolved in the GPC eluent at a concentration of 5 mg/mL and characterized by GPC analysis.

2.7. Animal experiments

All animal experiments were approved by local and national regulatory authorities and by an animal ethics welfare committee. CD-1 nude mice weighing 25-30 g were fed chlorophyll-free food and water ad libitum. Animals were hosted in ventilated cages under controlled temperature and humidity. CT26 colon carcinoma cells (ATCC) were cultured in Dulbecco's modified eagle's medium (DMEM; Invitrogen, Germany) supplemented with 10% fetal bovine serum (FBS; Invitrogen, Germany) and 1% Pen/strep (mixture of 10,000 U/mL penicillin and 10,000 μg/mL streptomycin) at 37 °C and 5% CO_2. Mice were subcutaneously inoculated with $1*10^6$ CT26 tumor cells in 100 μl medium in their right flank. Tumor growth was monitored three times weekly, and as soon as the average tumor diameter reached a size of 6-8 mm, the imaging experiments were initiated.

2.8. In vivo imaging

Anesthetized mice bearing 6-8 mm-sized CT26 tumors were placed in a multi-modal imaging cassette and high-resolution dual-energy micro-CT imaging was performed using a Tomoscope DUO (CT-Imaging, Erlangen, Germany). Images with an isotropic voxel size of 35 μm were reconstructed using a modified Feldkamp algorithm with a smooth kernel. Immediately after the micro-CT scan, the animals were transferred to the FMT2500 device (PerkinElmer, Rodgau, Germany) using the multimodal mouse cartridge which tightly holds the mice in a fixed position. iCCPM were administered at a dose of 2 nanomoles. Initially, a whole body image of the mouse was captured using the FRI functionality of the FMT. Based on this image, the region of interest (ROI) was set and a 3D FMT scan was performed. The spatial density of scanning mode was set to 'medium', i.e. the 3 mm-default setting. Animals were pre-scanned to assess the background fluorescence level. CT-FMT imaging was carried out at several different time points, i.e. 1, 4, 24 and 48 h post injection. The FMT and CT data sets were fused by computing a rigid transformation using fiducial markers in the mouse cassette. Based on the CT data, tumors and several healthy were segmented using the Imalytics Preclinical Software (Philips, Aachen, Germany). The FMT signals were overlaid

onto the respective organ-segmented CT images, and probe accumulation (in picomoles) in tumors and healthy organs was quantified. The percentage of the injected dose (%ID) was calculated based on quantifications obtained for each segmented organ, and they were normalized to average organ volume at the corresponding time point.

2.9. Ex vivo imaging

Following the last imaging time point at 48 h, rhodamine-lectin was injected (to stain tumor blood vessels), and animals were sacrificed 15 min later. Tumor and several different healthy organs were excised, weighed and scanned *ex vivo* using FRI. Subsequently, organs were embedded in TissueTec, and cryosections were prepared for standard 2D fluorescence microscopy (FM) and 3D two-photon laser scanning microscopy (TPLSM). The tumor accumulation of Dy-488- and Dy-676-labeled CCPM was assessed in 8 μm thick sections, using an Axio Imager M2 microscope. FM images were post-processed using the AxioVision Rel 4.8 software (Carl Zeiss Microimaging GmbH, Gottingen, Germany). For TPLSM, cryosections were cut into 200 μm thick slices, and imaged using an Olympus FV1000MPE multiphoton microscopy system (Mai Tai DeepSee pulsed Ti:Sapphire femtosecond-laser) at an excitation wavelength of 800 nm and a 25× water dipping objective (Numeric Aperture = 1.05; Working Distance = 2 mm). Three photon multiplier tubes were used to detect the fluorescence signals, and filters were adjusted to the corresponding spectra: 390-480 nm for second harmonic generation imaging of collagen fibers, 495-540 nm for Dy-488-labeled micelles and 595-650 nm for rhodamine-lectin stained blood vessels. TPLSM images were analyzed using the Imaris software (Bitplane, Zurich, Switzerland).

3. RESULTS AND DISCUSSION

3.1. Synthesis of mPEG-b-p(HPMAm-Lac-co-ANHS)

The block copolymer mPEG-b-p(HPMAm-Lac-co-ANHS) was synthesized by free radical polymerization of HPMAm-Lac and ANHS, initiated by a $mPEG_{5000}$ macroinitiator (Scheme 2A). The polymer was yielded with high conversion of both monomers (91% for HPMAm-Lac and 100% for ANHS). The M_n of the polymer (calculated by ^1H NMR) was 14 kDa, and correlated well with the value determined using GPC (16 kDa). The polydispersity of the block copolymer was 1.7.

3.2. Conjugation of Dy-488 and Dy-676 to mPEG-b-p(HPMAm-Lac-co-ANHS)

mPEG-b-p(HPMAm-Lac-co-ANHS) was coupled to either Dy-488 or Dy-676 (reaction between amine and NHS; Scheme 2 B-C). After a reaction time of 96 h, the coupling efficiencies of the Dy-488 and Dy-676 labeling were 51% and 56%, respectively. After the coupling reactions, on average, 3.1 and 3.8% of the polymer chains in each reaction were labeled with molecule of Dy-488 and Dy-676. The conjugation of the fluorophores to the polymer functionalized with NHS ester side groups was performed in a chemo-selective manner, in which amidation only occurs to NHS-activated ester groups, but in which the lactate ester groups do not react.

3.3 Preparation and characterizations of CCPM and iCCPM

Micelles were prepared using thermosensitive block copolymers via the rapid heating protocol.[15, 16, 37] The size of the NCPM, as determined using DLS, was 92 nm, with a low polydispersity index (PDI) of 0.07. mPEG-b-p(HPMAm-Lac-co-ANHS) was synthesized by free radical polymerization and the obtained polymer had a relatively high polydispersity index (Mw/Mn =1.7). However the polymeric micelles prepared using this polymer had a reasonable size (92 nm) and a low PDI (<0.1), which can be explained by the fact that even copolymers with relatively different molecular weights and architectures can self-assemble into micelles in a controlled manner. The CCPM were prepared by micelle crosslinking with cystamine (Scheme 2D). The size of the CCPM was comparable to that before crosslinking (94 nm with a PDI of 0.14). After four cycles of Vivaspin centrifugation, there were no HPLC-detectable amounts of free dyes in the filtrate, which means the non-conjugated free fluorophores were removed from the iCCPM by Vivaspin centrifugation. The emission spectra of the iCCPM excited at 491 nm (for Dy-488) and 674 nm (for Dy-676) were recorded, and the results confirm that both fluorophores were present in the iCCPM and were fluorescently active at 37 °C (Figure 1A-B). The size of the iCCPM was measured by nanoparticle tracking analysis (NTA), because the iCCPM absorbed the laser light of DLS (wavelength 488 nm). As shown in Figure 1C, in line with the size of the CCPM determined using DLS, the size of the iCCPM was 100 nm, and the SD was 30 nm, which points to a relatively narrow size distribution. [51] The zeta potential of the iCCPM was −0.6±0.11 mV, and slightly negative surface charge of the particles favors applications of them for intravenous injection. the These findings demonstrate that fluorophore-labeled and core-crosslinked polymeric micelles can be efficiently prepared using the rapid heating method, without using organic solvents for precipitation and dialysis. As opposed to the radical polymerization of methacrylate-containing side groups in the micellar core [31, 30, 32], cystamine-based core-crosslinking is thus shown to be compatible with Dy-488 and Dy-676.

3.4 Stability, integrity and de-crosslinking of CCPM

The stability of the CCPM was evaluated using three different approaches. First, the thermal stability of the NCPM and CCPM was examined by DLS while cooling the micellar dispersion. The light scattering intensity of the polymer dissolved in PBS 7.4 at low temperature (5 °C) was measured and this value was found to be 21±4. This light scattering value was considered as the baseline for other DLS measurements. Due to the thermosensitivity of mPEG-b-p(HPMAm-Lac-co-ANHS), the NCPM completely dissociated by lowering the temperature to 2 °C, as exemplified by the light scattering intensity decreasing to less than 5% of that at observed 25 °C (Figure 2A). The NCPM showed similar temperature-responsiveness as other non-crosslinked polymeric micelles with similar composition.[15, 30] The CCPM, on the other hand, displayed a relatively stable light scattering intensity upon cooling from 25 °C to 2 °C (Figure 2B), confirming the high stability of the CCPM upon cystamine-crosslinking. The size of the CCPM was found to be slightly increased upon cooling (~130 nm), which can be ascribed to rehydration and swelling of the micellar core at low temperatures. Upon accelerated hydrolysis (i.e. pH 10.0 and 37 °C), the NCPM showed a fast drop in the intensity of light scattering, to values below 5% of the original value within less than 1 h, suggesting a complete dissociation of

the NCPM via hydrolysis of the hydrophobic polymer side groups (Figure 2C).[16, 48] However, the scattering intensity of the CCPM only decreased with ~50% in 22 h, showing that the CCPM were stable even after the pendent lactate groups of the polymers were hydrolyzed (Figure 2D). It is therefore concluded that the integrity of the CCPM after hydrolysis was retained because of crosslinking of the micellar core.

Upon 22 h of accelerated hydrolysis, the CCPM were incubated with DTT. Figure 3 shows that almost instantaneously after addition of DTT the light scattering signals dropped to very low values demonstrating that the CCPM are de-crosslinked in a reductive environment, as has been described before for other disulfide-crosslinked micellar systems. [52, 53]

The NCPM could be completely dissolved in DMF. As demonstrated via gel permeation chromatography (GPC) with a refractive index (RI) detector, a high RI signal was observed for the NCPM (Figure 4). In contrast, the CCPM were not molecularly dissolved in DMF and were filtered out by the pre-column before entering the GPC column. However, also the CCPM displayed a certain RI signal in GPC at the same polymer concentration (~20% of that of the NCPM; Figure 4), which can be ascribed to a small fraction of free polymer chains present in the final micellar dispersion. The GPC chromatogram of the CCPM after incubation with DTT (5 mM) for 24 hours at 37 °C was shown in Figure 4 (green line), which is identical to that of NCPM, in terms of both retention time and intensity, and therefore it suggests that the CCPM can be fully reduced by DTT at biological temperature.

3.5. *In vivo* optical imaging of the biodistribution and tumor accumulation of iCCPM

The fluorophore-labeled iCCPM were intravenously injected into mice bearing EPR-prone CT26 tumors, and their biodistribution and tumor accumulation were non-invasively monitored using 3D CT-FMT. It has been previously reported that NCPM based on mPEG-b-p(HPMAm-Lac$_n$) show fast dissociation *in vivo* after i.v. injection.[30] Therefore, in this study, we only analyzed CCPM. As exemplified by Figure 5A, by means of anatomical CT imaging, tumors and several different healthy organs were manually pre-segmented, to more accurately allocate the fluorescence signals coming from the iCCPM to these tissues.[28] The accumulation of the micelles within the tumors was quantified, and as expected, an effective accumulation in target site was observed, with ~4% of the injected dose (ID) accumulating in tumors at 24 h post i.v. injection (Figure 5B-C). This value is in line with other published papers, in which the target site accumulation of micelles (as well as other nanocarriers) was evaluated using optical and radionuclide-based imaging techniques.[28, 43-48]

Figure 5C also provides feedback on the accumulation of the iCCPM in several different healthy tissues. The liver uptake of the iCCPM was found to be ~20% at 48 h p.i., which corresponds with previous reports, and results from clearance by the mononuclear phagocytic system (MPS).[54-57] In addition, a relatively prominent kidney accumulation was observed (~20% of the injection dose at 1 h). At early time points, also localization in bladder could be detected (~10% ID at 1 h), indicating that part of the labeled polymers were excreted renally. As shown in Figure 4, the micellar dispersion contained a certain amount of free polymer chains (i.e. non-core-crosslinked; with a molecular weight of 14 kDa), explaining localization in kidney and bladder. Retention of the signal in kidney at later

time points during follow-up is in line with this notion, as drug- and/or targeting ligand-modified macromolecular nanocarriers progressively accumulate in the kidney over time.[19, 54-58] This likely results from the initial glomeral filtration of polymeric nanocarrier materials with a size below ~45 kDa, followed by their (unspecific) retention in brush border membranes in the kidney.

In good correspondence with the CT-FMT results, FRI imaging indicated that the iCCPM most prominently accumulated in kidney, liver and tumor (Figure 6). In line with the kinetics of EPR-mediated drug targeting, the tumor accumulation of the micelles appeared to be progressively increasing over time (Figure 6A). At 48 h post i.v. injection, mice were sacrificed, tumors and several healthy tissues were excised, and the amounts of iCCPM deposited in these organs were visualized and quantified. As shown in Figures 6B-C, also *ex vivo*, the iCCPM were found to primarily accumulate in kidney and liver, followed by tumor.

3.6. *Ex vivo* analysis of tumor accumulation and penetration using 2D FM and 3D TPLSM

Upon sacrificing the animals and harvesting tissues, tumors were cryosectioned for 2D fluorescence microscopy (FM) and 3D two-photon laser scanning microscopy (TPLSM). As shown in Figure 7A, using appropriate filter sets, both fluorophores could be detected using FM, in general in the vicinity of rhodamine-lectin stained blood vessels (in red). In the majority of cases, a good co-localization between the Dy-488 (in green) and the Dy-676 (in yellow) fluorophore was observed. On some occasions, however, signals were only observed in one of the channels, indicating the presence of free block copolymer chains. These could either result from polymers which were not efficiently core-crosslinked (see section 3.1 and 3.5), or - more likely - from iCCPM which initially accumulated in tumors in the form of intact micelles, but were subsequently bio-degraded *in situ* as tumor present with a more reductive environment than healthy organs.[33, 59] Panels 7B-C exemplify the benefit of integrating TPLSM in drug targeting studies, showing the 3D distribution of the iCCPM in a 500 × 500 × 100 μm tumor slice, as well as a 2D z-stack image demonstrating the ability of TPLSM to quantitatively assess their intratumoral distribution. Figures 7D-E finally provide a 3D TPLSM image in which second harmonic generation (SHG) imaging was employed to visualize collagen fibers, indicating that the iCCPM penetrate relatively deeply into the tumor interstitium, and are distributed relatively homogenously within tumors. High-resolution visualization of double-labeled liposomes in deep tissues was previously performed by multispectral optoacoustic tomography (MSOT).[60] However, the TPLSM enables highly detailed studies on the impact of the extracellular matrix (ECM) on the distribution of drugs and drug delivery systems within tumors, and it facilitates studies in which therapies modulating the ECM are being evaluated. Importantly, for such 3D TPLSM studies, fluorophores with wavelengths below ~600 nm have to be employed (because of the principles of two-photon excitation), underlining the importance of labeling nanomedicines with two different fluorophores.

Europe PMC Funders Author Manuscripts

4. CONCLUSION

In summary, we here developed a strategy for labeling core-crosslinked polymeric micelles (CCPM) with two different fluorophores (i.e. Dy-488 and Dy-676). A mild, cystamine-based and reduction-sensitive core-crosslinking strategy was employed, and this was shown to be compatible with the covalent entrapment of the fluorophores. Upon extensive physicochemical characterization, the resulting image-guided CCPM (iCCPM) were i.v. injected into mice bearing CT26 tumors, and their biodistribution and tumor accumulation was monitored using several different optical imaging techniques. *In vivo* imaging using 3D CT-FMT and 2D FRI showed that the micelles accumulated reasonably efficiently in tumors, with ~4% of the injected dose present in tumors at 24 h p.i., and with apart from tumors, also prominent accumulation in kidney and liver. *Ex vivo* imaging using 2D FM and 3D TPLSM confirmed the extravasation of the micelles out of tumor blood vessels, as well as their penetration relatively deep into the tumor interstitium. These findings demonstrate that establishing protocols for labeling nanomedicines with two different fluorophores, and employing several different *in vivo* and *ex vivo* optical imaging techniques within the same experimental setup, might be highly useful for facilitating translational nanomedicine research.

5. Future perspective

Polymeric micelles are extensively utilized as targeted drug delivery systems for chemotherapy in (pre)clinical studies. However, a detailed assessment of their *in vivo* fate (biodistribution and tumor tissue localization) and a correlation between such information and the therapeutic response are still lacking. A methodology of labeling polymeric micelles with multiple fluorophores and using multimodal optical imaging techniques to acquire such information was established in the present article. In future studies, this correlation can be used to facilitate the understanding of the therapy mechanism and further prediction of the therapeutic response of chemotherapy with drug-loaded polymeric micelles, which will potentially progress towards personalized (nano-) chemotherapy.

ACKNOWLEDGEMENTS

The authors gratefully acknowledge financial support by the China Scholarship Council (CSC), by the European Research Council (ERC Starting Grant 309495: NeoNaNo), the European Commission (FP7: COST-Action TD1004: Nanotheragnostics), by the German Research Foundation (DFG: LA-2937/1-2), and by the Two-photon Imaging Core Facility at the Interdisciplinary Center for Clinical Research (IZKF) at RWTH Aachen University.

REFERENCES

1. Farokhzad OC, Langer R. Nanomedicine: developing smarter therapeutic and diagnostic modalities. Adv Drug Deliv Rev. 2006; 58:1456–9. [PubMed: 17070960]
2. Peer D, Karp JM, Hong S, Farokhzad OC, Margalit R, Langer R. Nanocarriers as an emerging platform for cancer therapy. Nat Nano. 2007; 2:751–60.
3. Lammers T, Hennink WE, Storm G. Tumour-targeted nanomedicines: principles and practice. Br J Cancer. 2008; 99:392–7. [PubMed: 18648371]
4. Lammers T, Kiessling F, Hennink WE, Storm G. Drug targeting to tumors: Principles, pitfalls and (pre-) clinical progress. J Control Release. 2012; 161:175–87. [PubMed: 21945285]

5. Jain RK, Stylianopoulos T. Delivering nanomedicine to solid tumors. Nat Rev Clin Oncol. 2010; 7:653–64. [PubMed: 20838415]
6. Sumer B, Gao J. Theranostic nanomedicine for cancer. Nanomedicine. 2008; 3:137–40. [PubMed: 18373419]
7. Torchilin V. Tumor delivery of macromolecular drugs based on the EPR effect. Adv Drug Deliv Rev. 2011; 63:131–5. [PubMed: 20304019]
8. Deng C, Jiang Y, Cheng R, Meng F, Zhong Z. Biodegradable polymeric micelles for targeted and controlled anticancer drug delivery: Promises, progress and prospects. Nano Today. 2012; 7:467–80.
9. Jones M-C, Leroux J-C. Polymeric micelles-a new generation of colloidal drug carriers. Eur J Pharm Biopharm. 1999; 48:101–11. [PubMed: 10469928]
10. Kataoka K, Harada A, Nagasaki Y. Block copolymer micelles for drug delivery: Design, characterization and biological significance. Adv Drug Deliv Rev. 2012; 64(Supplement):37–48.
11. Oerlemans C, Bult W, Bos M, Storm G, Nijsen JF, Hennink W. Polymeric Micelles in Anticancer Therapy: Targeting, Imaging and Triggered Release. Pharm Res. 2010; 27:2569–89. [PubMed: 20725771]
12. O'Reilly RK, Hawker CJ, Wooley KL. Cross-linked block copolymer micelles: functional nanostructures of great potential and versatility. Chem Soc Rev. 2006; 35:1068–83. [PubMed: 17057836]
13. Read ES, Armes SP. Recent advances in shell cross-linked micelles. Chem Commun. 2007:3021–35.
14. van Nostrum CF. Covalently cross-linked amphiphilic block copolymer micelles. Soft Matter. 2011; 7:3246–59.
15. Shi Y, van den Dungen ETA, Klumperman B, van Nostrum CF, Hennink WE. Reversible addition-fragmentation chain transfer synthesis of a micelle-forming, structure reversible thermosensitive diblock copolymer based on the *N*-(2-hydroxy propyl) methacrylamide backbone. ACS Macro Letters. 2013; 2:403–8.
16. Shi Y, van Steenbergen MJ, Teunissen EA, Novo Ls, Gradmann S, Baldus M, et al. Π–Π stacking increases the stability and loading capacity of thermosensitive polymeric micelles for chemotherapeutic drugs. Biomacromolecules. 2013; 14:1826–37. [PubMed: 23607866]
17. Talelli M, Hennink WE. Thermosensitive polymeric micelles for targeted drug delivery. Nanomedicine. 2011; 6:1245–55. [PubMed: 21929459]
18. Wei H, Cheng SX, Zhang XZ, Zhuo RX. Thermo-sensitive polymeric micelles based on poly(N-isopropylacrylamide) as drug carriers. Prog Polym Sci. 2009; 34:893–910.
19. Lammers T, Subr V, Ulbrich K, Hennink WE, Storm G, Kiessling F. Polymeric nanomedicines for image-guided drug delivery and tumor-targeted combination therapy. Nano Today. 2010; 5:197–212.
20. Lammers T, Aime S, Hennink WE, Storm G, Kiessling F. Theranostic Nanomedicine. Acc Chem Res. 2011; 44:1029–38. [PubMed: 21545096]
21. Papagiannaros A, Kale A, Levchenko TS, Mongayt D, Hartner WC, Torchilin VP. Near infrared planar tumor imaging and quantification using nanosized Alexa 750-labeled phospholipid micelles. Int J Nanomedicine. 2009; 4:123. [PubMed: 19516891]
22. Zhang R, Lu W, Wen X, Huang M, Zhou M, Liang D, et al. Annexin A5–conjugated polymeric micelles for dual SPECT and optical detection of apoptosis. J Nucl Med. 2011; 52:958–64. [PubMed: 21571801]
23. Gao X, Cui Y, Levenson RM, Chung LWK, Nie S. In vivo cancer targeting and imaging with semiconductor quantum dots. Nat Biotech. 2004; 22:969–76.
24. Janib SM, Moses AS, MacKay JA. Imaging and drug delivery using theranostic nanoparticles. Adv Drug Deliv Rev. 2010; 62:1052–63. [PubMed: 20709124]
25. Ding H, Wu F. Image guided biodistribution and pharmacokinetic studies of theranostics. Theranostics. 2012; 2:1040–53. [PubMed: 23227121]
26. Xing Y, Zhao J, Conti PS, Chen K. Radiolabeled nanoparticles for multimodality tumor imaging. Theranostics. 2014; 4:290–306. [PubMed: 24505237]

27. Yen SK, Padmanabhan P, Selvan ST. Multifunctional iron oxide nanoparticles for diagnostics, therapy and macromolecule delivery. Theranostics. 2013; 3:986–1003. [PubMed: 24396508]
28. Kunjachan S, Gremse F, Theek B, Koczera P, Pola R, Pechar M, et al. Noninvasive optical imaging of nanomedicine biodistribution. ACS Nano. 2012; 7:252–62. [PubMed: 23067565]
29. Gremse F, Theek B, Kunjachan S, Lederle W, Pardo A, Barth S, Lammers T, Naumann U, Kiessling F. Absorption reconstruction improves biodistribution assessment of fluorescent nanoprobes using hybrid fluorescence-mediated tomography. Theranostics. Accepted.
30. Rijcken CJ, Snel CJ, Schiffelers RM, van Nostrum CF, Hennink WE. Hydrolysable core-crosslinked thermosensitive polymeric micelles: synthesis, characterisation and in vivo studies. Biomaterials. 2007; 28:5581–93. [PubMed: 17915312]
31. Talelli M, Iman M, Varkouhi AK, Rijcken CJF, Schiffelers RM, Etrych T, et al. Core-crosslinked polymeric micelles with controlled release of covalently entrapped doxorubicin. Biomaterials. 2010; 31:7797–804. [PubMed: 20673684]
32. Crielaard BJ, Rijcken CJ, Quan L, van der Wal S, Altintas I, van der Pot M, et al. Glucocorticoid-loaded core-cross-linked polymeric micelles with wailorable release kinetics for targeted therapy of rheumatoid arthritis. Angew Chem Int Ed. 2012; 51:7254–8.
33. Meng F, Hennink WE, Zhong Z. Reduction-sensitive polymers and bioconjugates for biomedical applications. Biomaterials. 2009; 30:2180–98. [PubMed: 19200596]
34. Rösler A, Vandermeulen GWM, Klok H-A. Advanced drug delivery devices via self-assembly of amphiphilic block copolymers. Adv Drug Deliv Rev. 2012; 64:270–9.
35. Ryu J-H, Chacko RT, Jiwpanich S, Bickerton S, Babu RP, Thayumanavan S. Self-cross-linked polymer nanogels: a versatile nanoscopic drug delivery platform. J Am Chem Soc. 2010; 132:17227–35. [PubMed: 21077674]
36. Sun H, Meng F, Cheng R, Deng C, Zhong Z. Reduction-sensitive degradable micellar nanoparticles as smart and intuitive delivery systems for cancer chemotherapy. Expert Opin Drug Deliv. 2013; 10:1109–22. [PubMed: 23517599]
37. Yang Y, Pan D, Luo K, Li L, Gu Z. Biodegradable and amphiphilic block copolymer – doxorubicin conjugate as polymeric nanoscale drug delivery vehicle for breast cancer therapy. Biomaterials. 2013; 34:8430–43. [PubMed: 23896006]
38. Duangjai A, Luo K, Zhou Y, Yang J, Kopeček J. Combination cytotoxicity of backbone degradable HPMA copolymer gemcitabine and platinum conjugates toward human ovarian carcinoma cells. Eur J Pharm Biopharm. 2014; 87:187–196. [PubMed: 24316339]
39. Zhang R, Luo K, Yang J, Sima M, Sun Y, Janát-Amsbury MM, Kopečeka J. Cover image Synthesis and evaluation of a backbone biodegradable multiblock HPMA copolymer nanocarrier for the systemic delivery of paclitaxel. J Control Release. 2013; 166:66–74. [PubMed: 23262201]
40. Luo K, Yang J, Kopečková P, Kopeček J. Biodegradable Multiblock Poly[N-(2-hydroxypropyl)methacrylamide] via Reversible Addition-Fragmentation Chain Transfer Polymerization and Click Chemistry. Macromolecules. 2011; 44:2481–8. [PubMed: 21552355]
41. Yang J, Luo K, Pan H, Kopečková P, Kopeček J. Synthesis of Biodegradable Multiblock Copolymers by Click Coupling of RAFT-Generated HeterotelechelicPolyHPMA Conjugates. Reactive & functional polymers. 2011; 71:294–302. [PubMed: 21499527]
42. Wong SY, Putnam D. Overcoming limiting side reactions associated with an NHS-activated precursor of polymethacrylamide-based polymers. Bioconjugate Chem. 2007; 18:970–82.
43. Neradovic D, Soga O, Van Nostrum CF, Hennink WE. The effect of the processing and formulation parameters on the size of nanoparticles based on block copolymers of poly(ethylene glycol) and poly(N-isopropylacrylamide) with and without hydrolytically sensitive groups. Biomaterials. 2004; 25:2409–18. [PubMed: 14741606]
44. Li Y, Lokitz BS, Armes SP, McCormick CL. Synthesis of reversible shell cross-linked micelles for controlled release of bioactive agents. Macromolecules. 2006; 39:2726–8.
45. Xu X, Smith AE, Kirkland SE, McCormick CL. Aqueous RAFT synthesis of pH-responsive triblock copolymer mPEO-PAPMA-PDPAEMA and formation of shell cross-linked micelles. Macromolecules. 2008; 41:8429–35.
46. Zhang J, Jiang X, Zhang Y, Li Y, Liu S. Facile fabrication of reversible core cross-linked micelles possessing thermosensitive swellability. Macromolecules. 2007; 40:9125–32.

47. Neradovic D, van Steenbergen MJ, Vansteelant L, Meijer YJ, van Nostrum CF, Hennink WE. Degradation mechanism and kinetics of thermosensitive polyacrylamides containing lactic acid side chains. Macromolecules. 2003; 36:7491–8.

48. Soga O, van Nostrum CF, Ramzi A, Visser T, Soulimani F, Frederik PM, et al. Physicochemical characterization of degradable thermosensitive polymeric micelles. Langmuir. 2004; 20:9388–95. [PubMed: 15461534]

49. Meng F, Hennink WE, Zhong Z. Reduction-sensitive polymers and bioconjugates for biomedical applications. Biomaterials. 2009; 30:2180–98. [PubMed: 19200596]

50. Novo L, van Gaal EVB, Mastrobattista E, van Nostrum CF, Hennink WE. Decationized crosslinked polyplexes for redox-triggered gene delivery. J Control Release. 2013; 169:246–56. [PubMed: 23583705]

51. Filipe V, Hawe A, Jiskoot W. Critical Evaluation of Nanoparticle Tracking Analysis (NTA) by NanoSight for the Measurement of Nanoparticles and Protein Aggregates. Pharmaceutical Research. 2010; 27:796–810. [PubMed: 20204471]

52. Jia Z, Wong L, Davis TP, Bulmus V. One-pot conversion of RAFT-generated multifunctional block copolymers of HPMA to doxorubicin conjugated acid- and reductant-sensitive crosslinked micelles. Biomacromolecules. 2008; 9:3106–13. [PubMed: 18844406]

53. Kakizawa Y, Harada A, Kataoka K. Environment-sensitive stabilization of core-shell structured polyion complex micelle by reversible cross-linking of the core through disulfide bond. J Am Chem Soc. 1999; 121:11247–8.

54. Allmeroth M, Moderegger D, Biesalski B, Koynov K, Rösch F, Thews O, Zentel R. Modifying the body distribution of hpma-based copolymers by molecular weight and aggregate formation. Biomacromolecules. 2011; 12:2841–9. [PubMed: 21692523]

55. Allmeroth M, Moderegger D, Gündel D, Buchholz H-G, Mohr N, Koynov K, Rösch F, Thews O, Zentel R. PEGylation of HPMA-based block copolymers enhances tumor accumulation in vivo: A quantitative study using radiolabeling and positron emission tomography. J Control Release. 2013; 172:77–85. [PubMed: 23954630]

56. Allmeroth M, Moderegger D, Gündel D, Koynov K, Buchholz H-G, Mohr K, Rösch F, Zentel R, Thews O. HPMA-LMA copolymer drug carriers in oncology: an in vivo pet study to assess the tumor line-specific polymer uptake and body distribution. Biomacromolecules. 2013; 14:3091–101. [PubMed: 23962188]

57. Borgman MP, Coleman T, Kolhatkar RB, Geyser-Stoops S, Line BR, Ghandehari H. Tumor-targeted HPMA copolymer-(RGDfK)-(CHX-A″-DTPA) conjugates show increased kidney accumulation. J Control Release. 2008; 132:193–9. [PubMed: 18687371]

58. Kunjachan S, Pola R, Gremse F, Theek B, Ehling J, Moeckel D, Hermanns-Sachweh B, Pechar M, Ulbrich K, Hennink WE, Storm G, Lederle W, Kiessling F, Lammers T. Passive versus active tumor targeting using RGD- and NGR-modified polymeric nanomedicines. Nano Letters. 2014; 14(2):972–81. [PubMed: 24422585]

59. Kuppusamy P, Li H, Ilangovan G, Cardounel AJ, Zweier JL, Yamada K, Krishna MC, Mitchell JB. Noninvasive imaging of tumor redox status and its modification by tissue glutathione levels. Cancer Res. 2002; 62:307–12. [PubMed: 11782393]

60. Lozano N, Al-Jamal WT, Taruttis A, et al. Liposome-gold nanorod hybrids for high-resolution visualization deep in tissues. J Am Chem Soc. 2012; 134:13256–13258. [PubMed: 22852749]

Europe PMC Funders Author Manuscripts

EXECUTIVE SUMMARY

- In the present study, a strategy that enables facile core-labeling of polymeric micelles with fluorophores has been developed, which is differentiated from many other synthesis schemes which uses ether harsh conditions for fluorophores conjugation or labels the corona of nanoparticles that may change circulation kinetics of nanoparticles in vivo.
- The polymeric micelles were readily crosslinked by cystamine, which ensures that the crosslinked micelles are degradable in vivo, in response to reduction environment of tumor tissues and/or cytoplasma.
- The hybrid technology of CT-FMT enables noninvasive assessment of biodistribution of the nanoparticles in vivo, with an improved accuracy compared to conventional optical imaging methods.
- The intratumoral distribution of the fluorophore-labeled polymeric micelles was revealed by two-photon laser scanning microscopy, which proves important information regarding the extravasation of the polymeric micelles.
- Overall, the current study established a synthesis strategy combining multimodal optical imaging techniques to accurately reveal distribution of polymeric nanoparticles in living objectives and localization details in tumors.

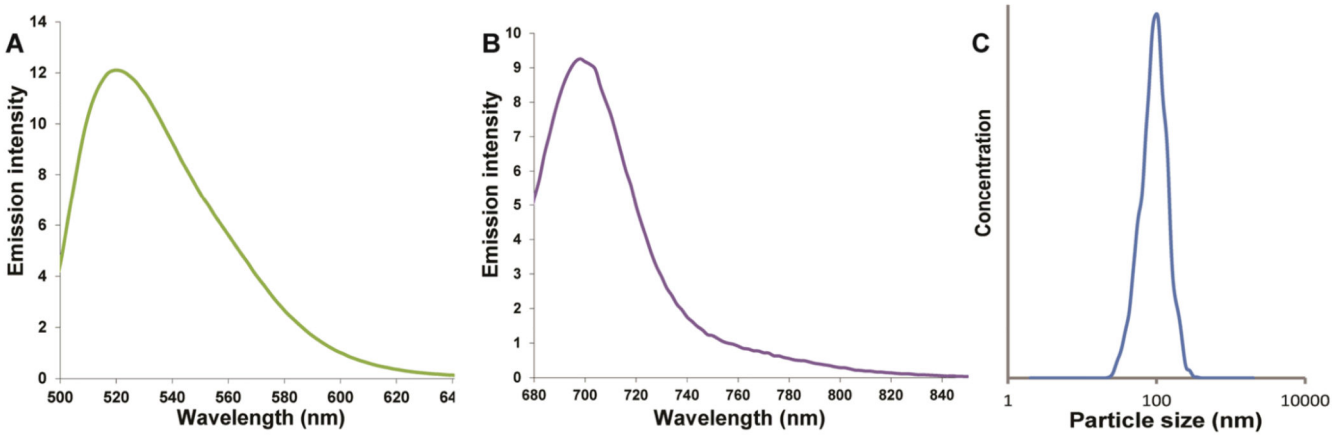

Figure 1.

A and B: Fluorescence emission spectra of iCCPM excited at 491 (A) and 674 (B) nm at 37 °C. C: Size distribution of the iCCPM as measured by nanoparticle tracking analysis (NTA)

Europe PMC Funders Author Manuscripts

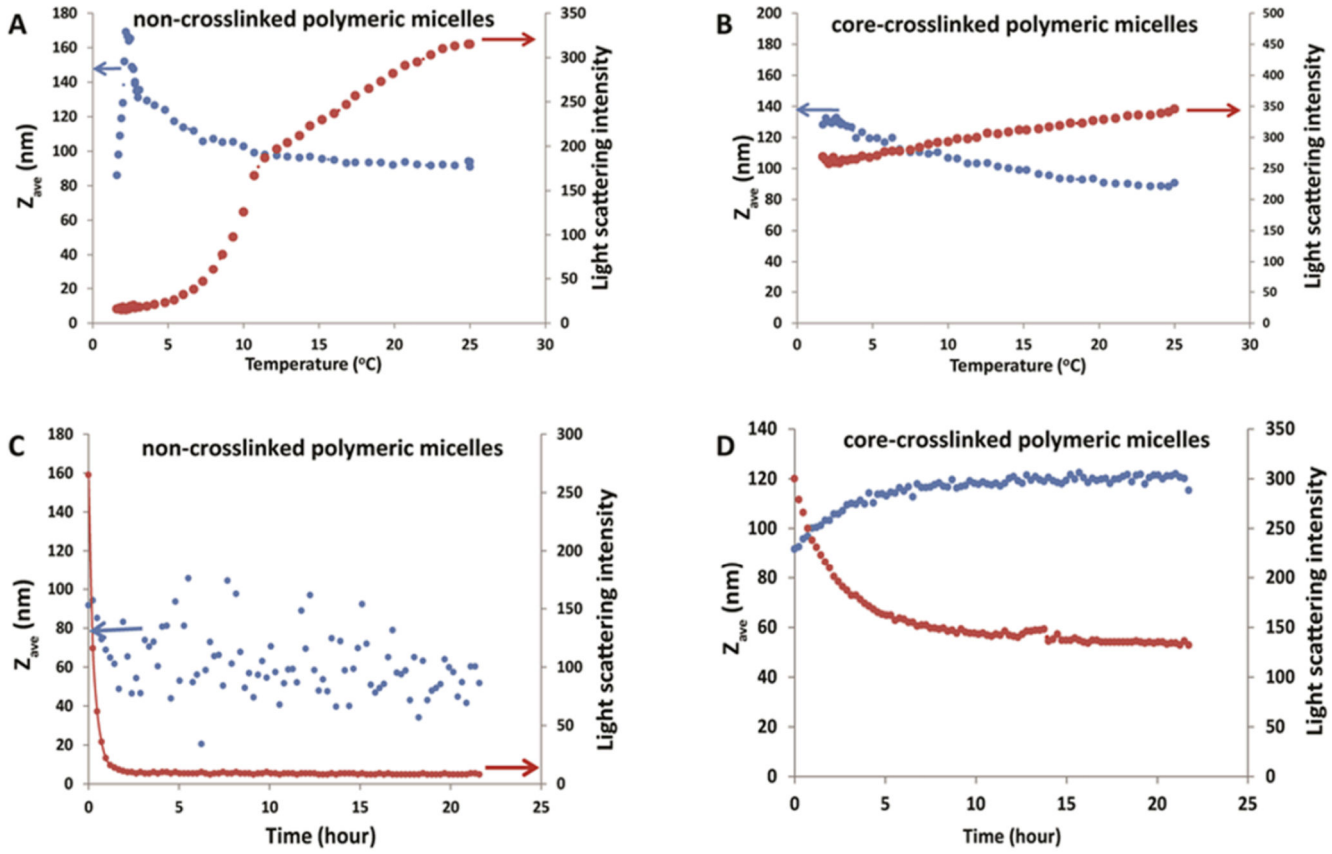

Figure 2.

A and B: Size and light scattering intensity of CCPM and NCPM while cooling the temperature-sensitive micelle formulations from 25 °C to 2 °C. The steady light scattering intensity of CCPM indicates good stability, while the significant drop in scattering intensity observed for NCPM indicates complete dissociation. C and D: Size and light scattering intensity of CCPM and NCPM upon accelerated hydrolysis (i.e. at pH 10 and 37 °C). The scattering of NCPM completed vanished, while that of CCPM was relatively stable

Europe PMC Funders Author Manuscripts

Europe PMC Funders Author Manuscripts

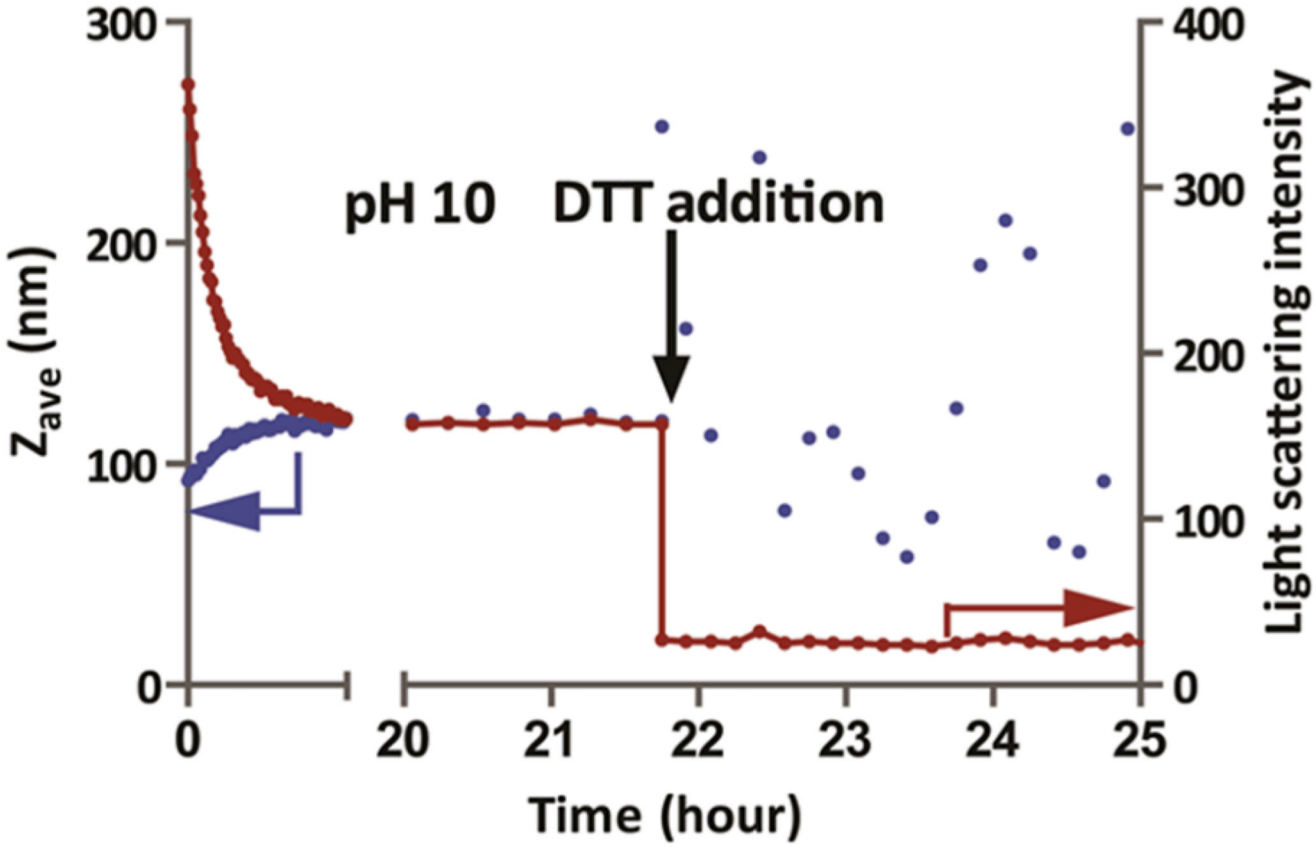

Figure 3.

Size and light scattering intensity of CCPM after accelerated hydrolysis (i.e. pH 10 and 37 °C) and additional DTT addition (to cleave the disulfide bonds). The light scattering intensity of the CPMM dramatically decreased upon DTT addition, confirming complete dissociation of the micelles

Europe PMC Funders Author Manuscripts

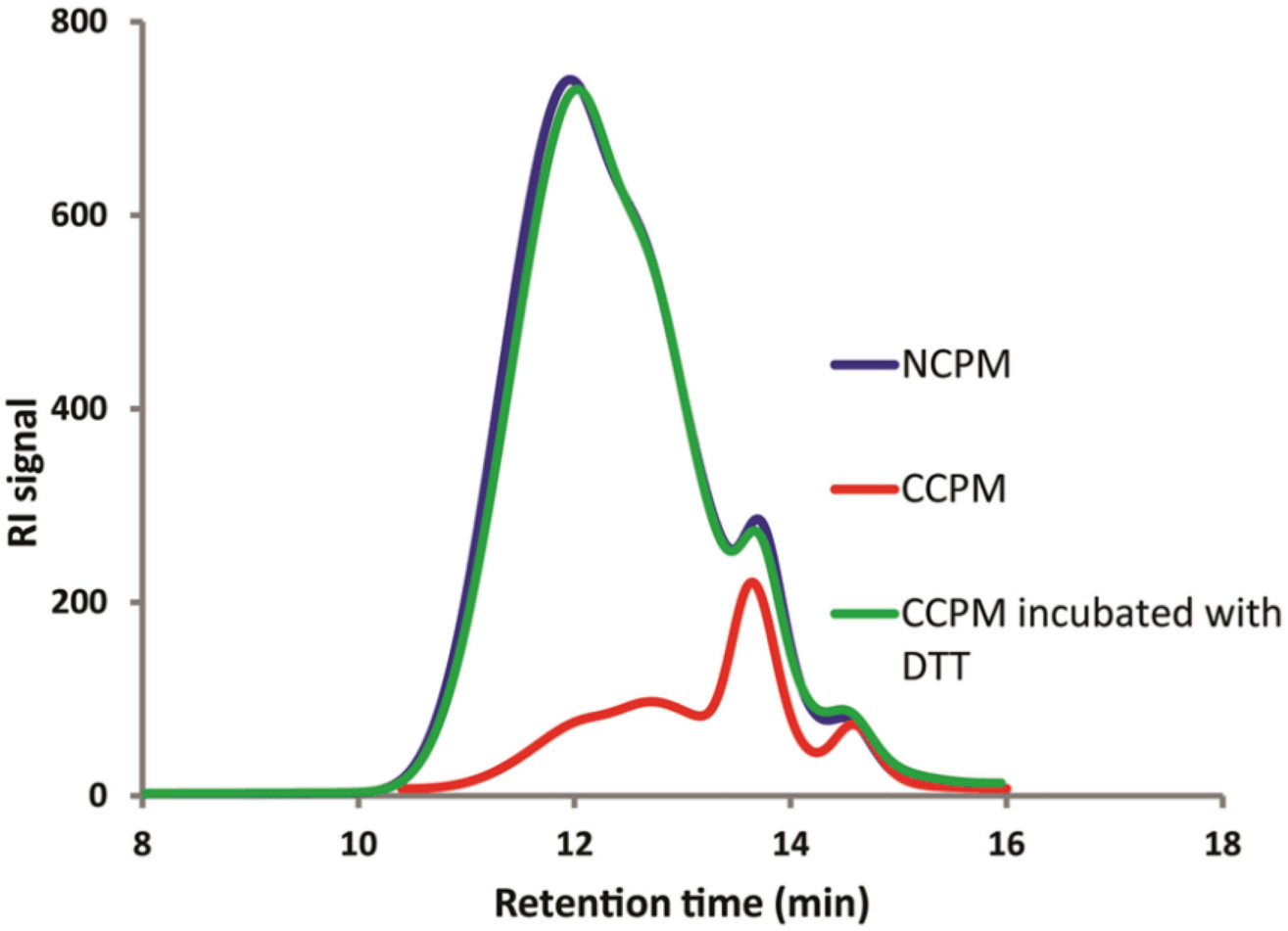

Figure 4.

GPC chromatograms of the NCPM and CCPM. NCPM were completely dissolved in DMF. CCPM also showed a certain refractive index (RI) signal, suggesting the presence of several free polymer chains within the final micellar dispersion

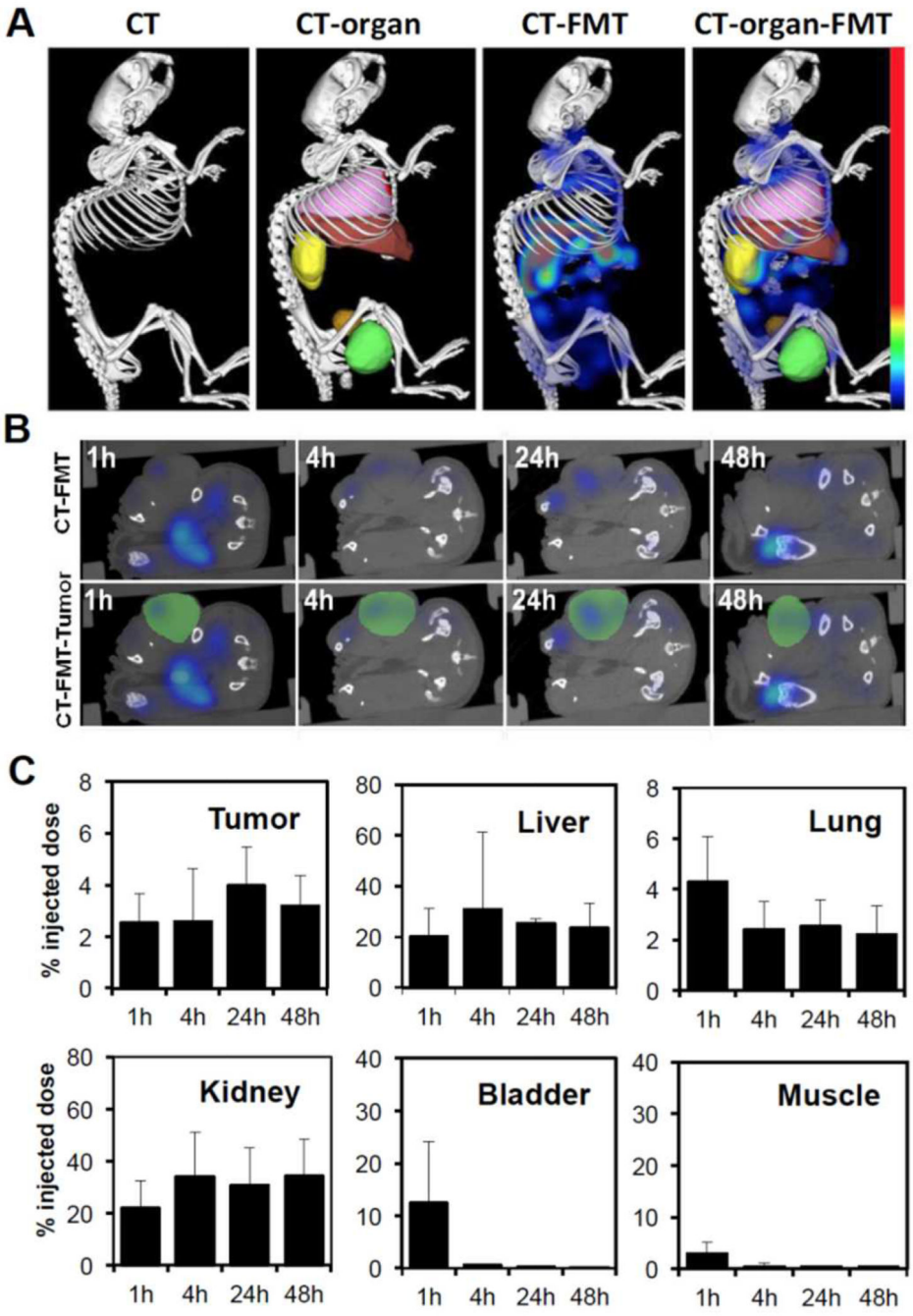

Figure 5.

Non-invasive in vivo CT-FMT imaging of the biodistribution and the tumor accumulation of iCCPM. The principle of hybrid CT-FMT imaging is shown in panel A, exemplifying that the anatomical information obtained using CT is used to assign the fluorescent signals coming from the iCCPM to a specific organ or tissue of interest. The images were obtained at 48 h p.i., and show probe localization in liver (brown), kidney (yellow) and tumor (green). Panels B and C confirm EPR-mediated accumulation of the iCCPM in tumors, with values reaching ~4% of the injected dose (%ID) at 24 h post i.v. injection. Panel C also provides

details on the accumulation of iCCPM in healthy organs. The reported percentages of the injected dose are normalized to average tissue volumes. Values represent average ± standard deviation (n=3)

Europe PMC Funders Author Manuscripts

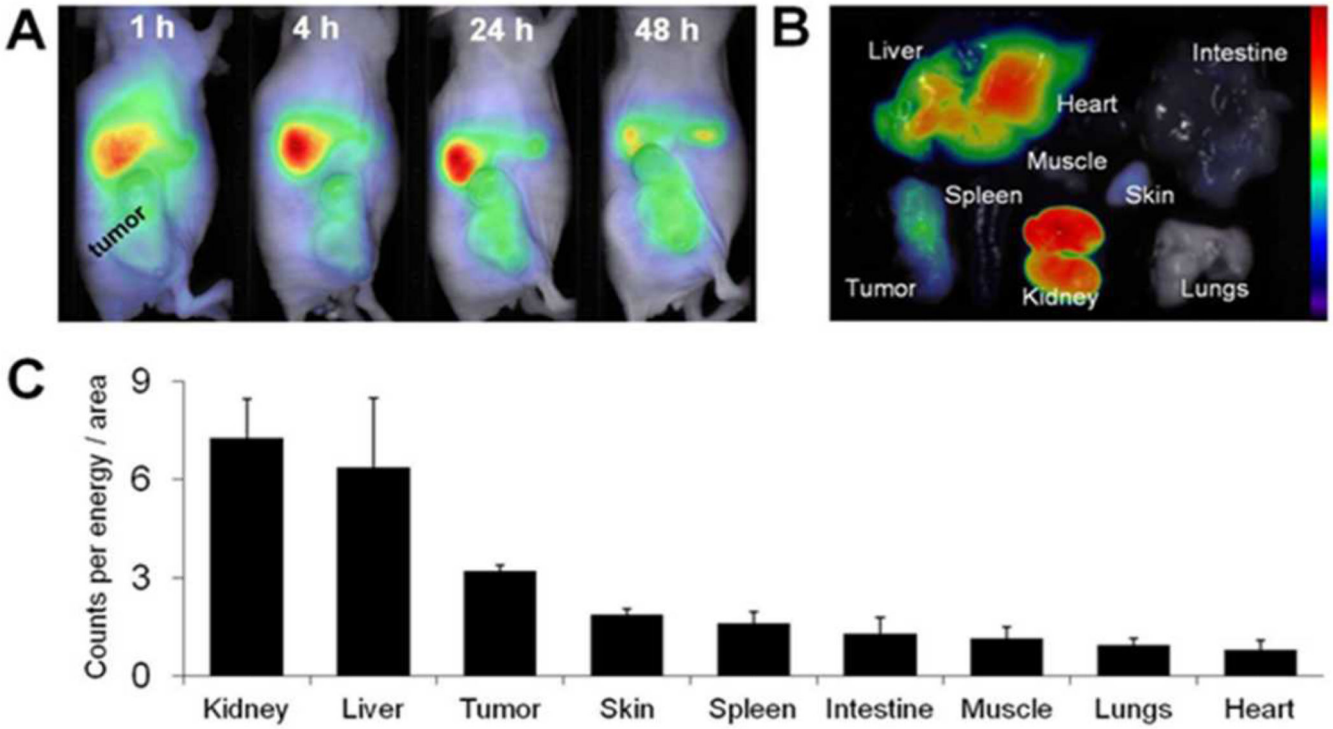

Figure 6.

In vivo (A) and ex vivo (B-C) FRI of iCCPM, exemplifying reasonably efficient EPR-mediated tumor targeting. Panel A hints toward accumulation in kidney, liver and tumor. This is confirmed via ex vivo imaging of excised organs (B-C), depicting the accumulation of the iCCPM in tumors and healthy organs at 48 h post i.v. injection. Values represent average ± SD (n=3)

Europe PMC Funders Author Manuscripts

Europe PMC Funders Author Manuscripts

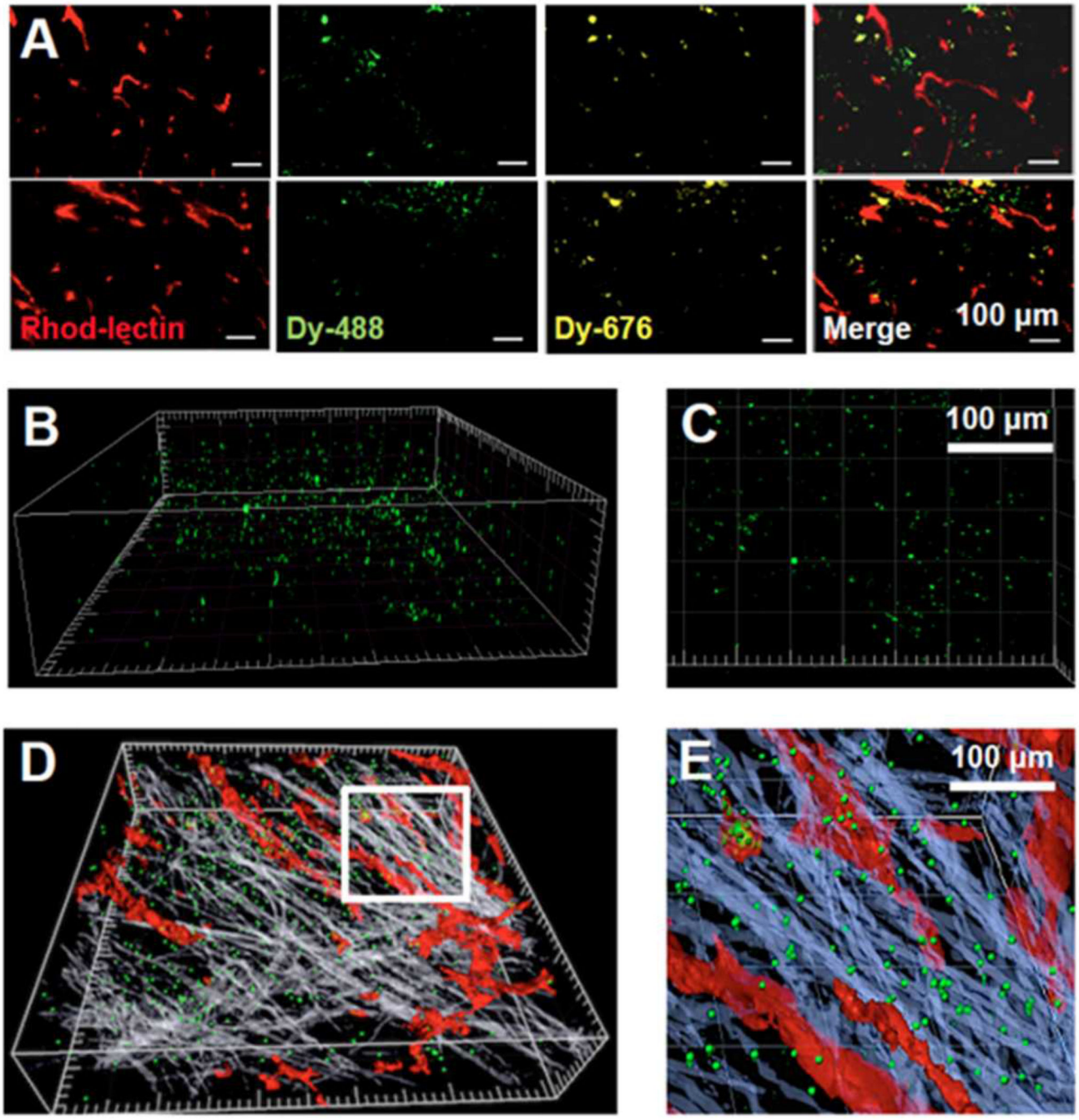

Figure 7.

Ex vivo analysis of the tumor accumulation of iCCPM using 2D FM and 3D TPLSM. Panel A shows representative fluorescence microscopy (FM) images of tumor sections with blood vessels stained in red (rhodamine-lectin) and with both fluorophores present within the iCCPM co-localizing in the majority of cases. Panels B-E are obtained using two-photon laser-scanning microscopy (TPLSM), and show that the iCCPM (green) efficiently extravasate from rhodamine-lectin-stained blood vessels (red), penetrate relatively deeply into the tumor interstitium, and are distributed relatively homogenously within tumors. The

grey and blue structures in panels D-E depict collagen fibers, visualized using second-harmonic generation (SHG) imaging

Europe PMC Funders Author Manuscripts

Europe PMC Funders Author Manuscripts

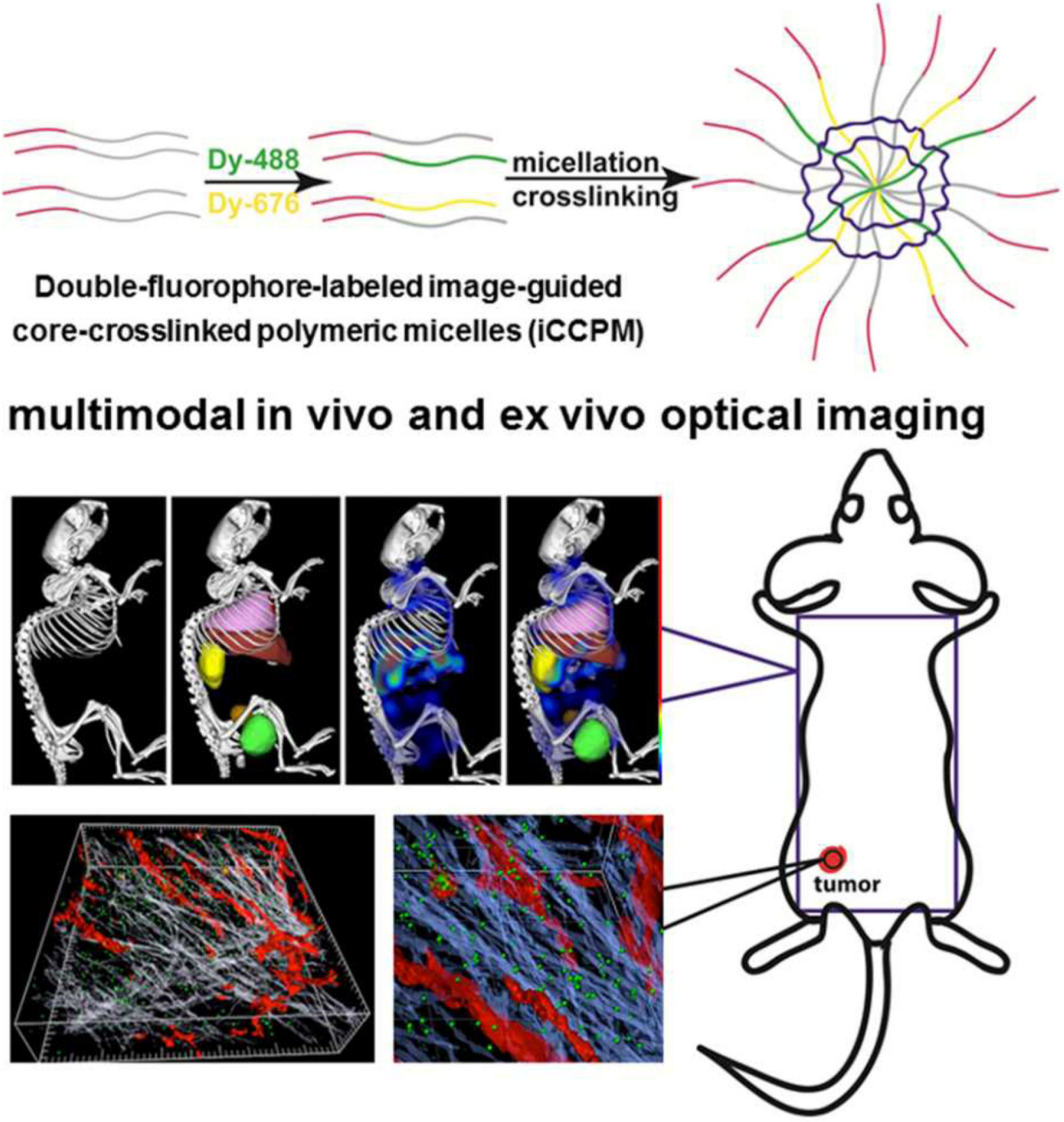

Scheme 1.

Core-crosslinked mPEG-b-p(HPMAm-Lac)-based polymeric micelles were labeled with two different fluorophores, and their biodistribution and tumor accumulation were analyzed using several different optical imaging techniques.

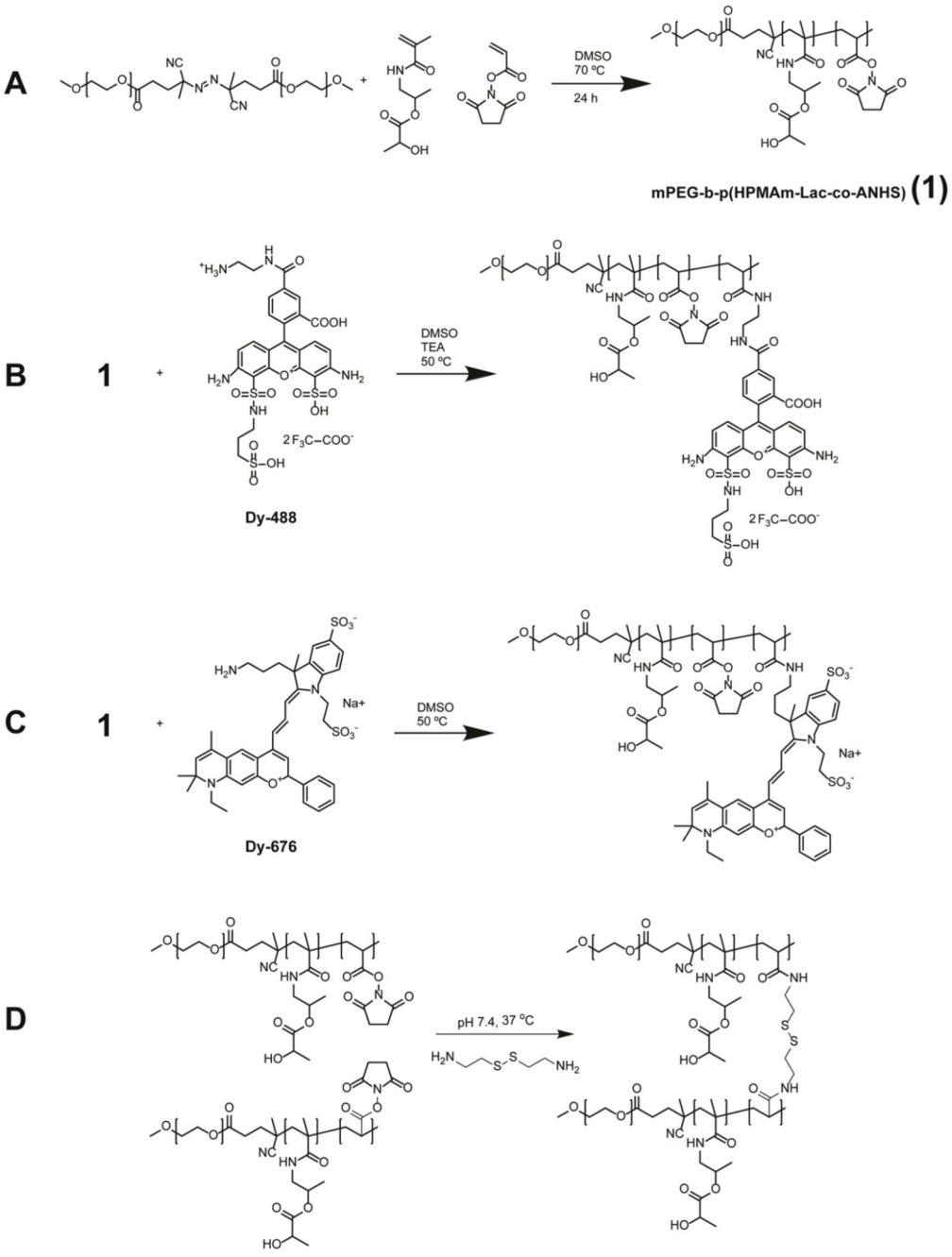

Scheme 2.

Synthesis of mPEG-b-p(HPMAm-Lac-co-ANHS (A)), conjugation of Dy-488 and Dy-676 (B and C) and crosslinking of the polymer chains (D)

Europe PMC Funders Author Manuscripts